Investigation of Spatial Harmonic Magnetic Field Coupling Effect on Torque Ripple for Multiphase Induction Motor Under Open Fault Condition

Wubin Kong, *Member, IEEE*, Min Kang, Dawei Li, *Member, IEEE*, Ronghai Qu, *Senior Member, IEEE*, Dong Jiang, *Senior Member, IEEE*, and Chun Gan, *Member, IEEE*

***Abstract*—This paper investigates spatial harmonic magnetic field coupling effect on torque ripple for multiphase induction motor under open fault condition. The coupling results in severe torque ripple generated by ellipse asynchronous magnetomotive force, and the current space vectors are utilized for coupling phenomenon analysis in the multiple planes. The optimal current space vector is proposed to achieve the minimum torque ripple, and the traditional method is used for comparison. Both fundamental and harmonic current space vectors are derived, when single-phase and two-phase open fault conditions are analyzed, respectively. Furthermore, the proportional integral resonant controller is used to realize zero-error tracking, and proper values of parameters in the transfer function are derived. Finally, a five-phase variable speed drive system is constructed and the proposed method is validated by experiments.**

***Index Terms*—Current space vector, open fault, proportional integral resonant (PIR), space harmonic magnetic field coupling, torque ripple.**

I. Introduction

IN HIGH-POWER application, the multiphase motor system is recognized as an alternative solution to obtain high-power ratings without increasing phase current, and the standard power devices can be fully adopted without parallel structure [1], [2]. Multiphase induction motor (IM) systems have competitive advantages for inherent robustness, reliability, high torque density, and low cost [3], [4]. The pace of research started accelerating in the 1990s, predominantly due to the developments in the area of electric ship propulsion, which remains nowadays one of the main application areas for multiphase variable-speed drives [5]. A different solution is however used in conjunction with high-power synchronous motors for pumps and compressors [6]. Nowadays, the multiphase motor drive is also used in the aerospace and electric vehicle (EV) application [7], [8].

Multiphase IM obtains additional degrees of freedom compared to three-phase motor, and it can be exploited in various ways. According to magnetomotive force (MMF) analysis under healthy condition, a general n-phase system can be decomposed into (n–1)/2 independent space vector in different planes, and the zero-sequence component [9]–[12]. Compared with three-phase motors, multiphase motor with additional control freedom can realize fault-tolerant operation. The remaining phase current can be also optimized to compensate the fault and continue torque-ripple free operation [13], [14]. Under open phase fault, the solution for fault-tolerant currents is not unique due to additional degrees of freedom. The general fault control for multiphase motor is solved by reconstructing the residual stator currents to generate circular rotating MMF as healthy condition [15], [16]. Another method for fault-tolerant control introduces the general decoupled model of multiphase motor with up to (n–3) open phases [17]–[19]. The fault-tolerant control strategy aims to reduce torque ripple under fault condition, when the minimum stator copper loss or the same stator currents is realized by additional control freedom [20].

In general, the torque ripple is generated due to the asymmetry in the stator mutual inductances, rotor currents, and stator currents. This topic is discussed in [1]–[4] and [15]–[22], and the several fault tolerant control strategies with different optimal goals, in terms of minimum stator copper loss, the same stator current, and minimum torque ripple, are illustrated in detail. Spatial harmonic magnetic field coupling is a crucial topic for torque-ripple analysis under fault condition, especially for multiphase motor with concentrated full-pitch winding. In ideal case of motors with sinusoidal distributed stator winding, the fundamental stator current space vectors do not contribute to spatial harmonic distribution of MMF [21]. On the contrary, each current space vector can produce ellipse rotating asynchronous MMFs for concentrated full-pitch winding, and it affects the motor torque ripple. The distinguished fault-tolerant control technique for five-phase permanent motor (PM) motor with trapezoid electromotive force (EMF) with optimized third

Manuscript received January 23, 2017; revised April 20, 2017 and June 10, 2017; accepted July 31, 2017. Date of publication August 8, 2017; date of current version March 5, 2018. This work was supported by the National Natural Science Foundation of China under Projects 51607078, 51407161, and 51520105010. Recommended for publication by Associate Editor J. Hur. *(Corresponding Author: Dawei Li.)*

W. Kong, D. Li, R. Qu, and D. Jiang are with the State Key Laboratory of Advanced Electromagnetic Engineering and Technology, School of Electrical and Electronic Engineering, Huazhong University of Science and Technology, Wuhan 430074, China (e-mail: wubinkong@126.com; daweili@hust.edu.cn; ronghaiqu@hust.edu.cn; jiangdong.tsinghua@gmail.com).

M. Kang is with the School of Automation and Electrical Engineering, Zhejiang University of Science and Technology, Hangzhou 310023, China (e-mail: kkkmin@yeah.net).

C. Gan is with the Department of Electrical Engineering and Computer Science, University of Tennessee, Knoxville, TN 37996 USA (e-mail: cgan@utk.edu).

Color versions of one or more of the figures in this paper are available online at http://ieeexplore.ieee.org.

Digital Object Identifier 10.1109/TPEL.2017.2737027

harmonic current injection, and imbalance third harmonic current also improves torque density and minimizes the torque ripple [22]. Based on the analysis of star stator winding configuration, pentagon and pentacle stator windings are investigated to compare torque ripple performance with optimized third harmonic current injection [23], [24]. Control of seven-phase motor under open-circuit phase faults is presented and assessed, and minimum torque pulsation control strategy is analyzed by considering the first three spatial harmonics of the air-gap MMF [25]. However, the previous works lack comprehensive analysis for spatial harmonic magnetic field coupling problem, and essential principle for torque ripple reduction is not illustrated properly.

Regarding the type of current control under fault condition, some initial works proposed the use of hysteresis controllers with variable frequency [16]. Subsequent works focus on other approaches such as the synchronous frame current control with forward compensation, but the method is difficult to extend for other different phase motor [19]. As an alternative to the dominating trend of filed oriented control with linear proportional integral (PI) controllers, the predictive control has emerging as a promising competitor [26]. Many contributions have been made for three-phase and multiphase in the healthy condition [27], [28]. The predictive current method is also applied in the speed control of five-phase IM with integrated open-phase fault operation [29], [30], but this method requires high performance processor with additional cost. The development of more advanced control scheme has proved that dual-PI controller can be very effective in tracking asymmetry currents under fault condition [31]. Despite the main advantage of the latter method has been proved for withstanding fault situations, no thorough improved regulator has been done for fault-tolerant control.

In this paper, a novel fault-tolerant control method is investigated to achieve minimum torque ripple under open fault condition, which is based on the analysis of spatial harmonic magnetic field coupling phenomena. The current space vector is introduced to represent the degree of coupling, and residual stator currents are reconstructed for reducing torque pulsation and satisfying zero-neutral current constraint. According to current space vector representation, it can be seen that fundamental spatial plane is not orthogonal to harmonic spatial planes under fault condition. The reverse magnetic field in the fundamental spatial plane results in severe torque pulsation, and the proposed method is presented to achieve torque ripple free. Furthermore, the optimal current control for fundamental and harmonic current is realized by proportional integral resonant (PIR) regulator, and the values of proportional and integral time constant in the transfer function are also derived. Finally, the proposed method with optimized harmonic current injection is further validated by experiments.

II. Space Harmonic Magnetic Field Coupling Principle Analysis Under Open Fault Condition

A. Behavior of Five-Phase IM in the Healthy Condition

Multiphase motor with concentrated full-pitch winding usually utilizes harmonic current injection method to improve

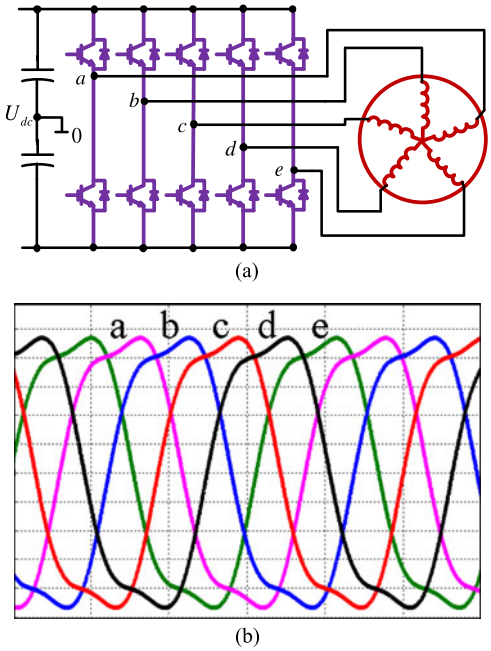

Fig. 1. Five-phase IM drive. (a) Topology of five-phase with single neutral point. (b) Five-phase stator current with third harmonic current injection.

operation [10]–[12], [15]. The typical isolated neutral, five-phase inverter in Fig. 1(a) is constructed to drive a star connected five-phase IM, and five-phase stator currents with third harmonic component are demonstrated in Fig. 1(b).

The five-phase motor through a set of four dependent variables divided into two orthogonal planes, namely, $\alpha_1 - \beta_1$ and $\alpha_3 - \beta_3$, and a zero sequence component [10]–[12], [16]. In the healthy condition, the generalized Clark transformation is given by [10]

$$[T_5] = \frac{2}{5}\begin{bmatrix} 1 & \cos(\gamma) & \cos(2\gamma) & \cos(3\gamma) & \cos(4\gamma) \\ 0 & \sin(\gamma) & \sin(2\gamma) & \sin(3\gamma) & \sin(4\gamma) \\ 1 & \cos(3\gamma) & \cos(6\gamma) & \cos(9\gamma) & \cos(12\gamma) \\ 0 & \sin(3\gamma) & \sin(6\gamma) & \sin(9\gamma) & \sin(12\gamma) \\ 1/2 & 1/2 & 1/2 & 1/2 & 1/2 \end{bmatrix} \begin{matrix} \rightarrow \boldsymbol{\alpha_1} \\ \rightarrow \boldsymbol{\beta_1} \\ \rightarrow \boldsymbol{\alpha_3} \\ \rightarrow \boldsymbol{\beta_3} \\ \rightarrow \mathbf{0} \end{matrix} \tag{1}$$

where $\gamma = 2\pi/5$. The orthogonal matrix (1) is used to transform stator quantities between *a–b–c–d–e* natural reference and $\alpha_1 - \beta_1 - \alpha_3 - \beta_3 - 0$ stationary reference frame.

Generally, third harmonic current is used for air-gap flux density optimization for five-phase IM. Under healthy condition, the five-phase stator currents with third harmonic currents are [16]

$$\begin{bmatrix} i_a \\ i_b \\ i_c \\ i_d \\ i_e \end{bmatrix} = \begin{bmatrix} i_{a1} \\ i_{b1} \\ i_{c1} \\ i_{d1} \\ i_{e1} \end{bmatrix} + \begin{bmatrix} i_{a3} \\ i_{b3} \\ i_{c3} \\ i_{d3} \\ i_{e3} \end{bmatrix} = \begin{bmatrix} I_1 \sin(\omega t) \\ I_1 \sin(\omega t - \gamma) \\ I_1 \sin(\omega t - 2\gamma) \\ I_1 \sin(\omega t - 3\gamma) \\ I_1 \sin(\omega t - 4\gamma) \end{bmatrix} + \begin{bmatrix} I_3 \sin(3\omega t) \\ I_3 \sin(3\omega t - 3\gamma) \\ I_3 \sin(3\omega t - 6\gamma) \\ I_3 \sin(3\omega t - 9\gamma) \\ I_3 \sin(3\omega t - 12\gamma) \end{bmatrix} \tag{2}$$

where I_1 is amplitude for the fundamental current, I_3 is amplitude for the third harmonic current, and ω is angular frequency.

When open fault occurs in the stator phase, the corresponding stator currents go down to zero. The fundamental current space vectors are

$$\left[\sum_{\rho=1,3}\sum_{k=1,3}\vec{i}^{k}_{S\rho}\right] = \left[\vec{i}^{1}_{S1}\right] + \left[\vec{i}^{3}_{S1}\right] + \left[\vec{i}^{1}_{S3}\right] + \left[\vec{i}^{3}_{S3}\right]$$
$$= [T_5]\left[\vec{i}_{abcde}\right] = [T_5]\left[\vec{i}_{a1b1c1d1e1}\right] + [T_5]\left[\vec{i}_{a3b3c3d3e3}\right] \quad (3)$$

where k represents the spatial number for plane, and ρ is time number for current.

B. Coupling Analysis Between Fundamental Plane and Third Harmonic Plane Under Open Fault

Obviously, $\vec{i}^{1}_{S1}$ is current space vector with fundamental current mapped into fundamental plane, and $\vec{i}^{3}_{S1}$ is current space vector with fundamental current mapped into third spatial harmonic plane. Similarly, $\vec{i}^{1}_{S3}$ and $\vec{i}^{3}_{S3}$ are the third harmonic current mapped into corresponding spatial planes. It can be turned out that the current $\vec{i}^{1}_{S1}$, $\vec{i}^{3}_{S1}$, $\vec{i}^{1}_{S3}$, and $\vec{i}^{3}_{S3}$ are not independent any more under open fault condition. Since the reference current space vector $\vec{i}^{1}_{S1}$ is the main component to generate the torque, and it should be maintained for the same trajectory. Thus, $\vec{i}^{3}_{S1}$ cannot be satisfied to be null, because the fundamental plane is coupled with third harmonic plane under fault condition. Unfortunately, the third harmonic current is also mapped into fundamental spatial plane with larger torque ripple, because $\vec{i}^{1}_{S3}$ is acted with fundamental plane inductance.

Under healthy condition, the fundamental current space vector is mapped into $d_1 - q_1$ plane only, and it is orthogonal to $d_3 - q_3$ plane. Similarly, third harmonic current space vector has the same characteristic, and the magnetic fields are displayed in Fig. 2(a). However, the fundamental spatial plane is coupled with third harmonic spatial plane under fault condition, and the magnetic field distribution is shown in Fig. 2(b). The fundamental current space vector produces two magnetic fields simultaneously, and the field rotating speed is $\pm\omega$ and $\pm\omega/3$, respectively. Meanwhile, the fundamental current in the third harmonic spatial plane generates torque ripple. Similarly, the third harmonic current space vector generates $\pm 3\omega$ and $\pm\omega$ rotating speed MMFs. However, the third harmonic current space vector produces larger torque ripple, because the value of inductance in the fundamental spatial plane is greater [9]–[11], [17].

In generation case, it is necessary to keep the first spatial harmonic undisturbed and to preserve the same $\vec{i}^{1}_{S1}$ as the healthy condition. The third harmonic current is also designed to remain the same current space vector $\vec{i}^{3}_{S3}$, as shown in the Fig. 3(a). The reverse rotating current space vectors is removed by fault-tolerant control, while $\vec{i}^{3}_{S1}$ and $\vec{i}^{1}_{S3}$ cannot be minimized to zero, and current space vector $\vec{i}^{3}_{S1}$ and $\vec{i}^{1}_{S3}$ generate asynchronous MMF. Reverse-rotating stator MMF generated by current space vectors should be avoided, because low-frequency torque ripple is an essential problem in the motor system. $\vec{i}^{1}_{S3}$ is acted with

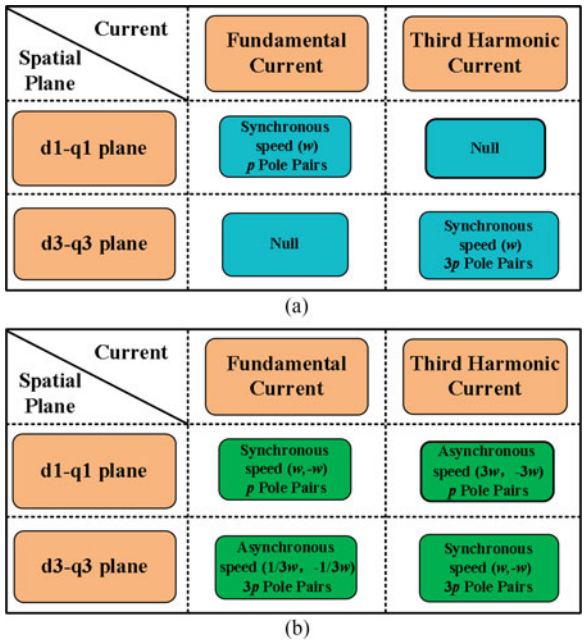

Fig. 2. Relationship between stator current and magnetic field. (a) Healthy condition. (b) Open-fault condition.

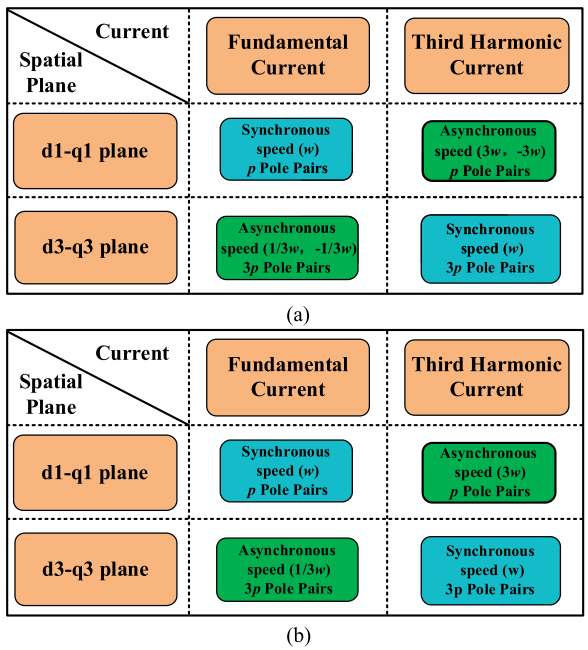

Fig. 3. Coupling analysis under one-phase open fault condition. (a) Traditional fault-tolerant method. (b) Proposed fault-tolerant method.

fundamental spatial plane with large inductance, while $\vec{i}^{3}_{S1}$ generates less torque pulsation in the third harmonic spatial plane with small inductance. $\vec{i}^{3}_{S1}$, $\vec{i}^{1}_{S3}$, and $\vec{i}^{3}_{S3}$ are optimized with novel stator currents in the proposed method. $\vec{i}^{1}_{S3}$ is designed to force the MMF mapped into fundamental spatial plane to move along forward circular trajectory, as shown in the Fig. 3(b).

Similarly, the coupling analysis for two-phase open fault condition is shown in the Fig. 4. There are only three phase remaining, and the control freedom is also reduced. Consequently, $\vec{i}^{3}_{S1}$ and $\vec{i}^{1}_{S3}$ can be realized circular trajectory simultaneously

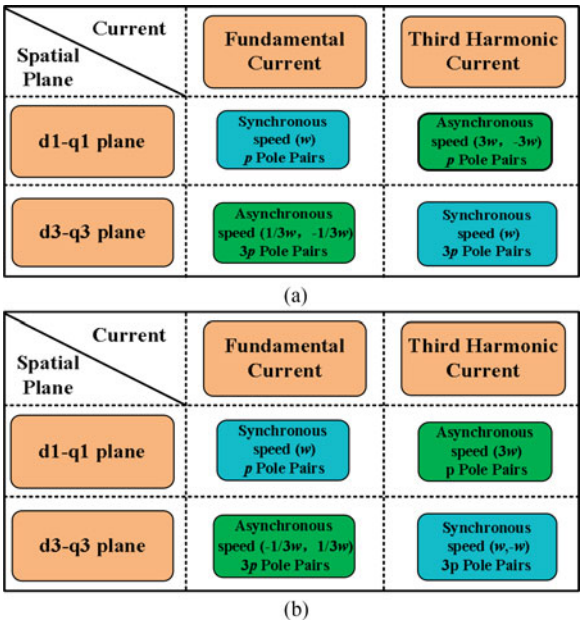

Fig. 4. Coupling analysis under two-phase open fault condition. (a) Traditional fault-tolerant method. (b) Proposed fault-tolerant method.

shown in Fig. 4(a). The current space vector $\vec{i}^{1}_{S3}$ is optimized for forward speed to reduce the torque ripple, as shown in Fig. 4(b).

III. Torque Ripple Reduction With Proposed Fault-Tolerant Control Strategy

A. Traditional Method Under Single-Phase Open Condition

Fault-tolerant control strategies have various criterions, the same stator current control method is adopted to compared with the proposed method. This result is not new, and it has been published in previous literature. The residual stator currents for fundamental component are [22]

$$\begin{cases} i'_{a1} = 0 \\ i'_{b1} = 1.382I_1\cos(\omega t - \pi/5) \\ i'_{c1} = 1.382I_1\cos(\omega t - 4\pi/5) \\ i'_{d1} = -1.382I_1\cos(\omega t - \pi/5) \\ i'_{e1} = -1.382I_1\cos(\omega t - 4\pi/5). \end{cases} \tag{4}$$

Substituting (4) into (3), the current space vector for fundamental current are defined as follows:

$$\begin{bmatrix} K^1_{1\alpha}\vec{i}^{1}_{S1\alpha,\mathrm{ref}} \\ K^1_{1\beta}\vec{i}^{1}_{S1\beta,\mathrm{ref}} \\ K^3_{1\alpha}\vec{i}^{1}_{S1\alpha,\mathrm{ref}} \\ K^3_{1\beta}\vec{i}^{1}_{S1\beta,\mathrm{ref}} \\ 0 \end{bmatrix} = \frac{2}{5}\begin{bmatrix} 1 & \cos(\gamma) & \cos(2\gamma) & \cos(3\gamma) & \cos(4\gamma) \\ 0 & \sin(\gamma) & \sin(2\gamma) & \sin(3\gamma) & \sin(4\gamma) \\ 1 & \cos(3\gamma) & \cos(6\gamma) & \cos(9\gamma) & \cos(12\gamma) \\ 0 & \sin(3\gamma) & \sin(6\gamma) & \sin(9\gamma) & \sin(12\gamma) \\ 1/2 & 1/2 & 1/2 & 1/2 & 1/2 \end{bmatrix} \times \begin{bmatrix} 0 \\ 0 \\ i'_{c1} \\ i'_{d1} \\ i'_{e1} \end{bmatrix} \tag{5}$$

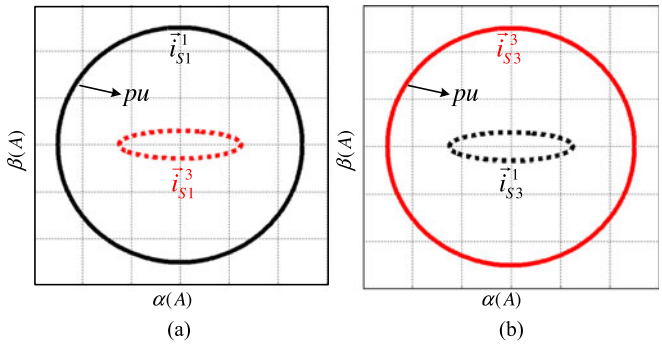

Fig. 5. Trajectories of current space vector under single-phase fault condition for the traditional method. (a) Fundamental stator current space vector. (b) Third harmonic stator current space vector.

where $\vec{i}^{1}_{S1\alpha,\mathrm{ref}} = \cos(\omega t)$, $\vec{i}^{1}_{S1\beta,\mathrm{ref}} = \sin(\omega t)$. The control strategy for same stator current amplitude, the coefficients are

$$K^1_{1\alpha} = 1.00\ K^1_{1\beta} = 1.00\ K^3_{1\alpha} = -0.50\ K^3_{1\beta} = 0.12\,. \tag{6}$$

Similarly, the third harmonic currents can be also derived [16] as follows:

$$\begin{cases} i'_{a3} = 0 \\ i'_{b3} = 3.618I_3\cos(3\omega t - 3\pi/5) \\ i'_{c3} = 3.618I_3\cos(3\omega t - 12\pi/5) \\ i'_{d3} = -3.618I_3\cos(3\omega t - 3\pi/5) \\ i'_{e3} = -3.618I_3\cos(3\omega t - 12\pi/5). \end{cases} \tag{7}$$

Similarly, substituting (7) into (3), the current space vector for third harmonic current are defined as follows:

$$\begin{cases} \vec{i}^{1}_{S3\alpha} = K^1_{3\alpha}\vec{i}^{1}_{S3\alpha,\mathrm{ref}} \\ \vec{i}^{1}_{S3\beta} = K^1_{3\beta}\vec{i}^{1}_{S3\beta,\mathrm{ref}} \\ \vec{i}^{3}_{S3\alpha} = K^3_{3\alpha}\vec{i}^{1}_{S3\alpha,\mathrm{ref}} \\ \vec{i}^{3}_{S3\alpha} = K^3_{3\beta}\vec{i}^{1}_{S3\alpha,\mathrm{ref}} \end{cases} \tag{8}$$

where $\vec{i}^{1}_{S3\alpha,\mathrm{ref}} = \cos(3\omega t)$ and $\vec{i}^{1}_{S3\beta,\mathrm{ref}} = \sin(3\omega t)$. The coefficients are

$$K^1_{3\alpha} = -0.50\ K^1_{3\beta} = 0.12\ K^3_{3\alpha} = 1.00\ K^3_{3\beta} = 1.00\,. \tag{9}$$

The current space vectors in (5) and (8) are demonstrated in the pattern of Lissajous trajectory. Fig. 3(a) demonstrates that $\vec{i}^{3}_{S1}$ is not null, and the trajectory is elliptical, and the reverse component can produce torque ripple, as shown in Fig. 5(a). Especially, $\vec{i}^{1}_{S3}$ with elliptical trajectory generates larger torque pulsation in the fundamental spatial plane in the Fig. 5(b).

B. Proposed Method Under Single-Phase Open Condition

The third harmonic currents above generate the same third harmonic magnetic field as the healthy condition, but the fundamental spatial plane cannot maintain zero simultaneously. The torque ripple cannot be neglected because of the larger value for inductance in the fundamental spatial plane. Hence, (4) and (7) are not proper values for minimum torque ripple. The mathematical model of a five-phase IM can be derived in terms of

multiple space vectors

$$R_r\vec{i}_{Rk}+\frac{d\vec{\varphi}_{Rk}}{dt}-jk\omega\vec{\varphi}_{Rk}=0,\quad (k=1,3) \tag{10}$$

$$\vec{\varphi}_{Rk}=L_{mk}\vec{i}_{Sk}+L_{Rk}\vec{i}_{Rk},\quad (k=1,3) \tag{11}$$

$$T_e=\frac{5}{2}P\sum_{\rho=1,3}\sum_{k=1,3}kL_{m\rho}\vec{i}_{Sk}\cdot j\vec{i}_{Rk} \tag{12}$$

where L_{mk} and L_{Rk} are the stator inductance and rotor inductance, respectively. The motor parameters are shown in the Table III.

The minimum torque ripple of (9) to the constraint can be given by the Lagrange multipliers method [31]. The stator currents are

$$\begin{cases} i'_{a1}=0 \\ i'_{b1}=1.902I_1\cos(\omega t-0.94) \\ i'_{c1}=1.179I_1\cos(\omega t-3.45) \\ i'_{d1}=1.179I_1\cos(\omega t-2.83) \\ i'_{e1}=1.902I_1\cos(\omega t-5.34). \end{cases} \tag{13}$$

The space vector for the fundamental currents can be derived as follows:

$$K^1_{1\alpha}=1.00\ K^1_{1\beta}=1.00\ K^3_{1\alpha}=0.50\ K^3_{1\beta}=0.50\,. \tag{14}$$

In this case, third harmonic currents can be calculated as

$$\begin{cases} i'_{a3}=0 \\ i'_{b3}=1.175I_3\cos(3\omega t-2.83) \\ i'_{c3}=1.901I_3\cos(3\omega t-0.94) \\ i'_{d3}=1.901I_3\cos(3\omega t-5.34) \\ i'_{e3}=1.175I_3\cos(3\omega t-3.45). \end{cases} \tag{15}$$

The space vector for the third harmonic currents can be derived as follows:

$$K^1_{3\alpha}=1.00\ K^1_{3\beta}=1.00\ K^3_{3\alpha}=0.50\ K^3_{3\beta}=0.50\,. \tag{16}$$

Reverse rotating MMF should be eliminated in order to reduce the torque pulsation under fault condition. As for five-phase IM drive under single-phase open condition, there are enough control freedoms to make $\vec{i}^1_{S1}$ and $\vec{i}^3_{S1}$ move along circular trajectories. The space vector behavior for the proposed method is depicted in Fig. 6. The space vector for fundamental and third harmonic currents both generate circular trajectories. Reverse rotating MMF is removed compared with the one in traditional method.

C. Two-Phase Open Condition

The maximum number of open phases for five-phase IM drive is up to two. These fault conditions can be divided into two groups, and the more serious fault condition for phase A and B open is analyzed in this section. The currents for open phase maintain zero, and the remaining stator currents can be derived for the same MMF distribution as healthy condition. It should be noted that there is no more control freedom to optimize two current space vectors simultaneously. There is unique solution for the fundamental stator currents, when it aims to maintain

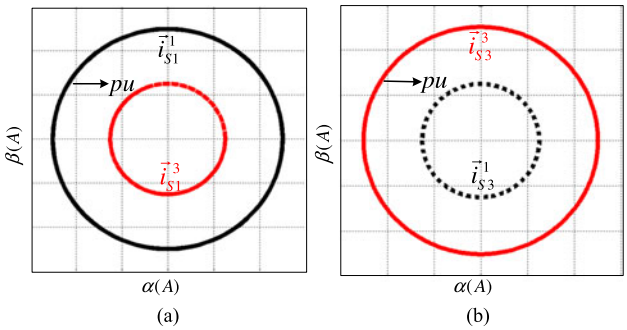

Fig. 6. Trajectories of current space vector under single-phase fault condition for the proposed method. (a) Fundamental stator current space vector. (b) Third harmonic stator current space vector.

the circular trajectory in the fundamental plane. Hence, the fundamental stator current expressions are the same between traditional method and proposed method. The expression are [16]

$$\begin{cases} i''_{a1}=0 \\ i''_{b1}=0 \\ i''_{c1}=2.236I_1\cos(\omega t-2\pi/5) \\ i''_{d1}=3.618I_1\cos(\omega t+4\pi/5) \\ i''_{e1}=2.236I_1\cos(\omega t). \end{cases} \tag{17}$$

The current space vectors for fundamental currents under two adjacent phase open fault are

$$K^1_{1\alpha}=1.00\ K^1_{1\beta}=1.00\ K^3_{1\alpha}=-0.28\ K^3_{1\beta}=-1.32\,. \tag{18}$$

The traditional method with third harmonic current injection is calculated in [16], and it achieves the object of circular current space vector in the third harmonic spatial plane. The third harmonic current expression is

$$\begin{cases} i''_{a3}=0 \\ i''_{b3}=0 \\ i''_{c3}=2.236I_3\cos(3\omega t-6\pi/5) \\ i''_{d3}=1.382I_3\cos(3\omega t+12\pi/5) \\ i''_{e3}=2.236I_3\cos(3\omega t). \end{cases} \tag{19}$$

The current space vectors for third harmonic currents with traditional method are as follows:

$$K^1_{3\alpha}=-0.28\ K^1_{3\beta}=-1.32\ K^3_{3\alpha}=1.00\ K^3_{3\beta}=1.00\,. \tag{20}$$

The third harmonic currents aim to maintain the circular trajectory in the fundamental spatial plane, while $\vec{i}^3_{S3}$ has reverse MMF trajectory. The inductance in the fundamental plane is nine-times as large as third harmonic plane, when the current space vector mapped into the fundamental plane with larger inductance according to the torque equation in (12). Hence, the trajectory of $\vec{i}^1_{S3}$ should be maintained circular. The third harmonic current is one control freedom, and it can be optimized

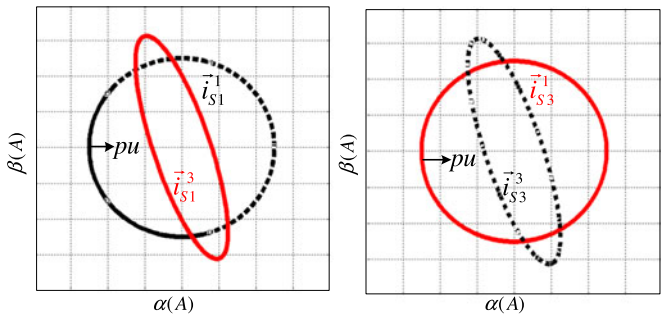

Fig. 7. Trajectories of current space vector under two-phase fault condition with proposed method. (a) Fundamental stator current space vector. (b) Third harmonic stator current space vector.

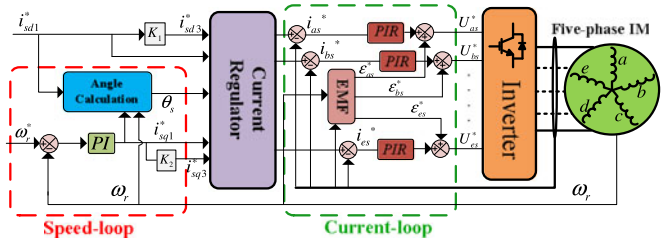

Fig. 8. Block diagram of fault-tolerant control scheme for five-phase IM drive.

to minimize the torque ripple with proper current space vector

$$\begin{cases} i''_{a3} = 0 \\ i''_{b3} = 0 \\ i''_{c3} = 2.236 I_3 \cos(3\omega t - 2\pi/5) \\ i''_{d3} = 3.618 I_3 \cos(3\omega t + 4\pi/5) \\ i''_{e3} = 2.236 I_3 \cos(3\omega t). \end{cases} \tag{21}$$

The current space vectors for third harmonic currents with proposed method are as follows:

$$K^1_{3\alpha} = 1.00 \; K^1_{3\beta} = 1.00 \; K^3_{3\alpha} = -0.28 \; K^3_{3\beta} = -1.32. \tag{22}$$

The space vector trajectory under two-phase open fault condition is demonstrated in Fig. 7. The trajectories mapped into fundamental spatial plane are circular, while the vectors in third harmonic spatial plane are elliptical. Hence, the proposed method can improve torque density and reduce torque ripple even under two-phase open fault condition.

IV. Fault-Tolerant Current Control Using Resonant Regulator

A. Fault-Tolerant Control in the Phase Frame

The control scheme for five-phase IM under fault condition is shown in Fig. 8, and it consists of speed-loop and current-loop. The reference current i^*_{sd1} maintains constant, and the third harmonic d-axis i^*_{sd3} is defined by coefficient K_1. The value of K_1 and K_2 is analyzed in [10]. The reference of i^*_{sq1} is determined by PI regulator on the basis of the speed error. Then, the stator current can be given by reverse park transformation, as shown in (4), (7), (13), and so on. The current loop can be realized by PIR current regulator, and the detail analysis is demonstrated in next section.

B. Proposed Resonant Controller and Parameter Tuning

For higher performance current regulation system, the residual reference tracking error is unacceptably large using PI regulator. In this situation, the only remaining alternative is to increase the gain of the forward controller block at the target reference frequency, but this would reduce the system phase stability margin. The forward gain block $G_c(s)$ of a practical proportional resonant (PR) control is described by the transfer function [27]

$$G_c(s) = k_p \left(1 + \frac{s}{\tau_i (s^2 + \omega_e^2)}\right) \tag{23}$$

where ω_e is the target reference frequency. $s/(s^2 + \omega_e^2)$ is resonant component for high gain in the forward loop.

Unfortunately, the ideal PR controller response defined by (23) can be challenging to physically realize, particularly using a fix-point calculation as is typically available in current generation digital signal process (DSP) with PWM capability. Hence, a more practical resonant controller is

$$G_c(s) = k_p \left(1 + \frac{s}{\tau_i (s^2 + \omega_r s + \omega_e^2)}\right) \tag{24}$$

where ω_r is the resonant cutoff frequency.

The PIR controller has better performance for bandwidth control, and it is suitable for realizing fundamental and third harmonic current tracking, when only one current regulator is applied for each phase. Since PIR controller phase reverts back to the PI controller at higher frequency, the k_p and integral gain τ_i can be used to optimized through PI controller [27].

As described in [28], the maximum cross frequency can be derived

$$\omega_{c(\max)} = \frac{\pi/2 - \phi_m}{T_d} \tag{25}$$

where ϕ_m is phase margin, and the value is usually set to $\pi/4$.

The integral time constant τ_i can be minimized by $\tan^{-1}(\omega_c \tau_i) \approx \pi/2$, and it can be given in the industrial application

$$\tau_i \approx \frac{10}{\omega_{c(\max)}}. \tag{26}$$

Then, the maximum possible magnitude of k_p can be derived by setting the open loop gain to unity

$$k_p \approx R_s \tau_i \omega_{c(\max)} \sqrt{\frac{(1 + \omega^2_{c(\max)} T_p^2)}{(1 + \omega^2_{c(\max)} \tau_i^2)}} \tag{27}$$

where R_s is the stator resistance for five-phase IM, and $T_p = (L_{os} + \frac{L_{or} L_m}{L_{or} + L_m})/R_s$. The stator leakage inductance L_{os} and rotor leakage inductance L_{or} are shown in the Table III.

Equations (23) and (24) show the mathematical derivation for the value of k_p and τ_i, which is crucial for the performance of PIR controller to ensure the system stability shown in the Fig. 8. According to mathematical analysis and simulation result, the

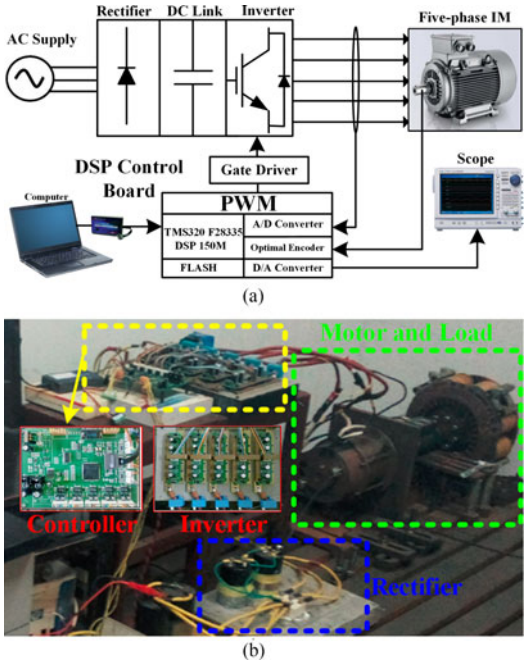

Fig. 9. Five-phase IM drive system. (a) Schematic diagram of the experimental platform. (b) Control system hardware and prototype motor.

controller gain $k_p = 0.80$ and $\tau_i = 0.00325$ s is applied in the current controller. Then, the mathematical expression in (24) can be used in further used in the current regulator in the Fig. 8.

V. Experimental Results and Discussion

A. System Implementation

The entire experimental setup for five-phase motor drive is shown in Fig. 9 and the experimental platform consists of five-phase voltage source inverter and control board. The five-phase IM with concentrated full pitch stator windings is shown in Fig. 9(b), whose nominal parameters of five-phase IM are shown in Appendix. The dc bus voltage is set for 72 V, and the power device consists of four MOSFET with parallel structure for each phase. The control algorithm is implemented in a DSP TMS320F28335 and the switching frequency is 10 kHz. The torque is tested by JN338 torque-speed sensor, and the response time of dynamic strain wave for strain gauge is 3.2×10^{-6} s. The output signal for torque-speed sensor ranges from 5 to 15 kHz, which represents the reverse and forward maximum torque, respectively. The torque waveform is transformed by F/V converter, and all the data captured from Yokogawa DL850 multiple-channel oscilloscope.

B. Single Open-Phase Fault

The results for optimized PIR control method with EMF compensation are demonstrated in Fig. 10. The current error is minimized distinctively at transient response. Hence, the comparative experimental results verify the effectiveness of PIR control method in the phase frame, and it achieves excellent current tracking even at fault occurrence.

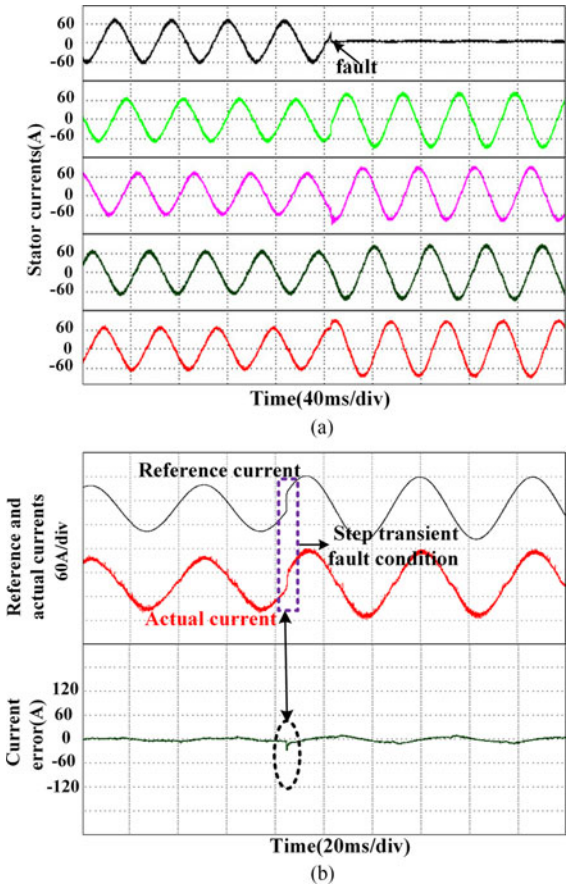

Fig. 10. Current tracking performance for PIR control method.

The boundary for fault condition is important, and the rest of phase currents should not exceed the rated values. The load should be decreased for long time operation, if thermal limit of phase winding and power electronic converter is taken into consideration. Preliminary experimental tests in the healthy condition are carried out at load torque of 16.0 N·m and a reference rotor speed of 300 r/min. The experimental results contains three components, including healthy condition, open fault condition, and fault-tolerant control condition. There is enough time for each stage, and the steady state and transient performance can be compared easily. In order to verify the effectiveness of the proposed method control strategy, four fault-tolerant control methods are compared, including the same amplitude for the stator currents without third harmonic current (M_1), the same amplitude for the stator currents with third harmonic current (M_2), minimum torque ripple without third harmonic current (M_3), and minimum torque ripple with third harmonic current (M_4). The M_1 and M_2 methods are the previous works in [16], and they are used to compare with the proposed method.

The experimental results for M_1 method is shown in Fig. 11. The torque is smooth in the healthy condition, while the torque pulsation increases up to 23.1% under open fault condition. The current space vector $\vec{i}_{S1}^{1}$ generates $-\omega$ and ω rotating MMFs. Thus, the frequency for torque ripple is 2ω, which is twice times as stator current frequency. The torque ripple is mainly caused by the reverse rotating MMF in the fault condition. The torque

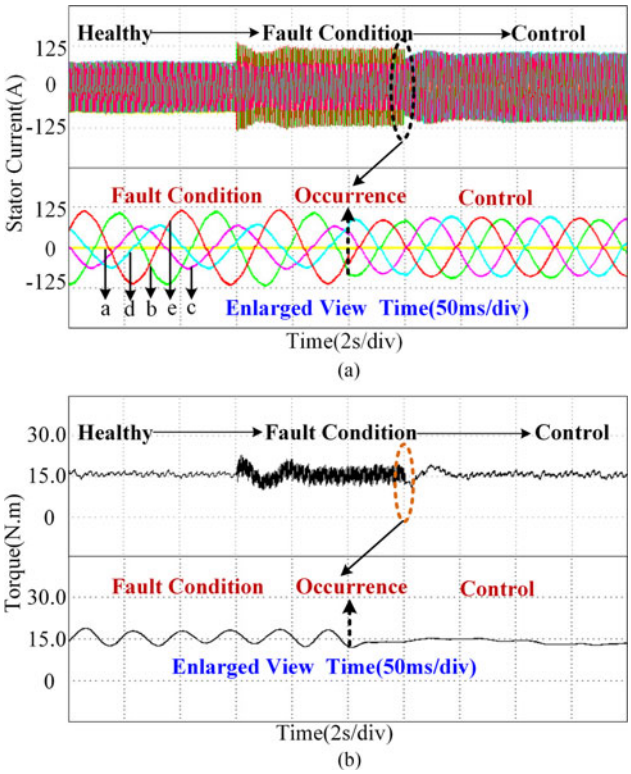

Fig. 11. Traditional method without third harmonic current injection (M_1 method). (a) Five-phase stator current. (b) Measured torque ripple.

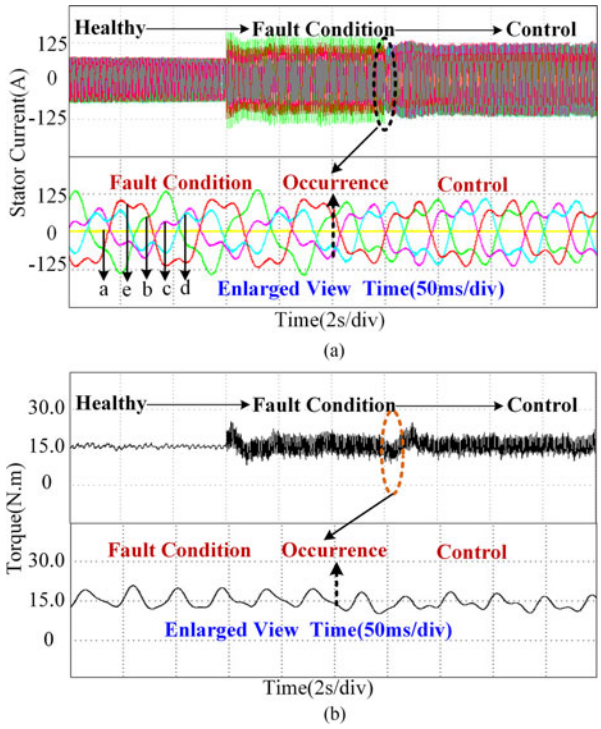

Fig. 12. Traditional method with third harmonic current injection (M_2 method). (a) Five-phase stator current. (b) Measured torque ripple.

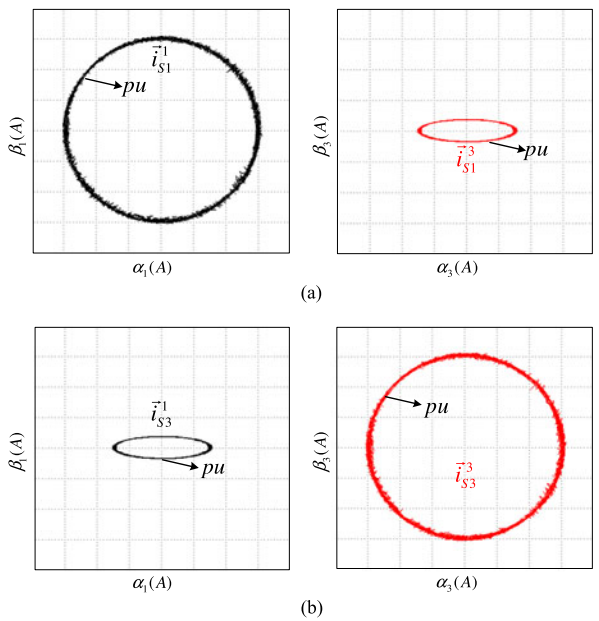

Fig. 13. Experimental results for the traditional method under single-phase fault condition. (a) Fundamental stator current space vector. (b) Third harmonic stator current space vector.

ripple is reduced significantly with fault-tolerant control strategy shown in Fig. 11(b).

The experimental results for M_2 method is shown in Fig. 12. Compared with M_1 method, third harmonic currents are injected into five-phase IM. However, the torque ripple still maintains large amplitude up to 20.2% under fault-tolerant control strategy. According to the analysis in Figs. 2 and 3, the current space vector $\vec{i}^{1}_{S3}$ generates $\pm 3\omega$ rotating MMF. They are acted with ω fundamental rotating MMF, and it will generate 2ω and -4ω angular frequency torque ripple. The torque ripple is mainly caused by third harmonic currents, which are coupled with the fundamental spatial plane. Furthermore, the current space vector for traditional method is shown in the Fig. 13, when the mathematical equation is demonstrated in (6) and (9). The current space vector $\vec{i}^{1}_{S3}$ is elliptical trajectory in the Fig. 13(b), and it generates the torque ripple in the Fig. 12(b).

The experimental results for M_3 method is shown in Fig. 14. This control strategy aims to the minimum torque ripple under fault condition. The torque waveform in Fig. 14(b) shows smooth performance, and it is similar with the healthy condition. Compared with M_1 method, this method has different amplitudes for the remaining stator currents.

The experimental results for M_4 method is shown in Fig. 15. Compared with M_3 method, the third harmonic currents are injected into five-phase IM. However, the torque ripple is still very small under fault-tolerant control condition. Hence, the results prove that the M_4 method reduces torque ripple obviously, when the third harmonic currents are utilized to improve the torque density. Compare with the M_2 method, the third harmonic currents are optimized to achieve torque ripple free performance. The current space vector results are shown in the Fig. 16, and all of them are maintained the circular trajectory with the proposed method. Hence, the torque ripple is reduced significantly compared with the traditional method (M_2).

To evaluate four fault-tolerant control strategies under single-phase open condition, two important parameters are presented.

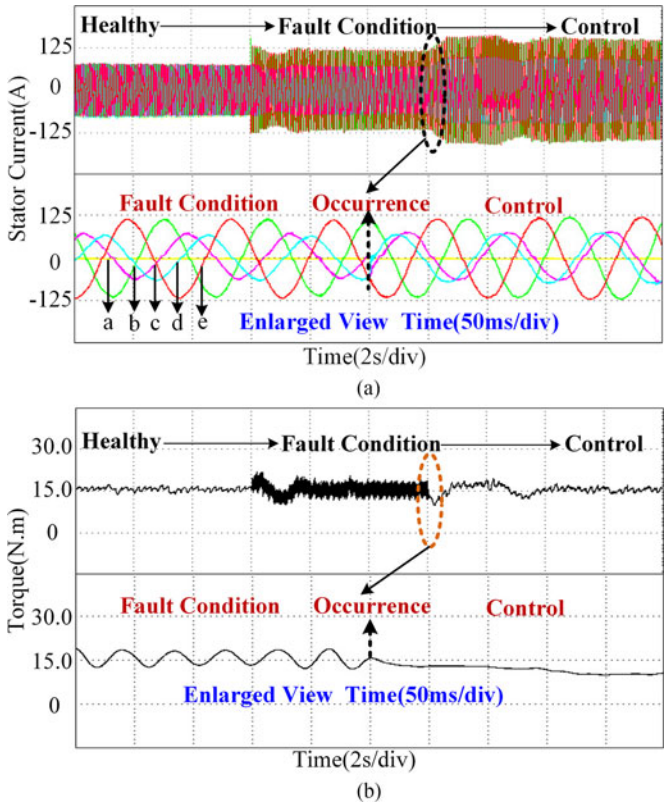

Fig. 14. Proposed method without third harmonic current injection (M_3 method). (a) Five-phase stator current. (b) Measured torque ripple.

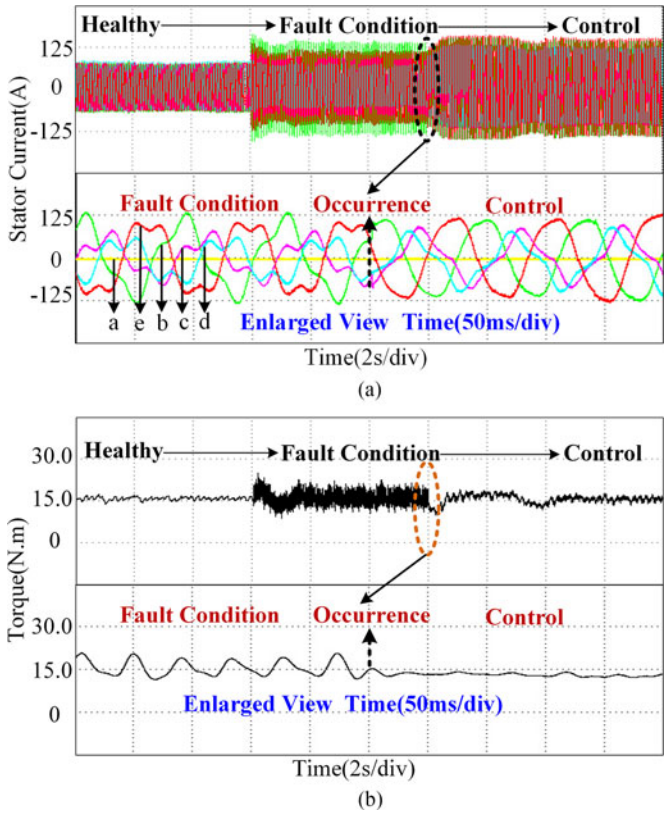

Fig. 15. Proposed method with third harmonic current injection (M_4 method). (a) Five-phase stator current. (b) Measured torque ripple.

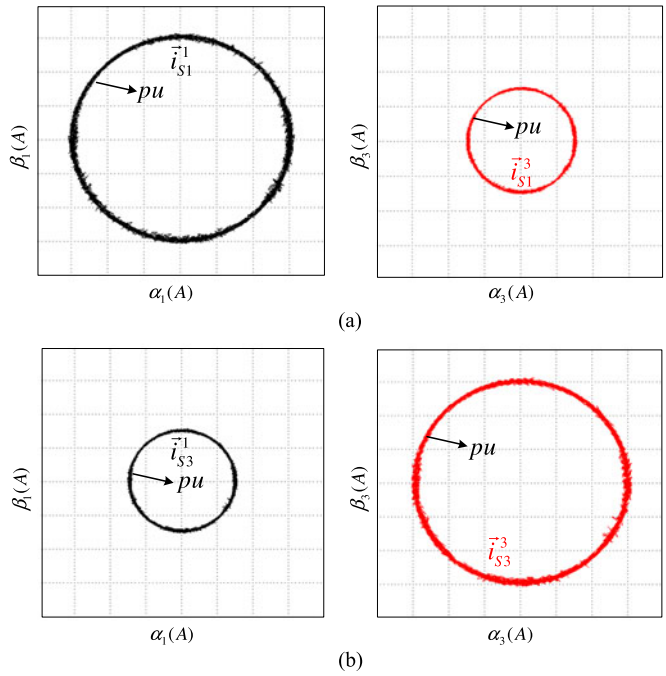

Fig. 16. Experimental results for the proposal method under single-phase fault condition. (a) Fundamental stator current space vector. (b) Third harmonic stator current space vector.

TABLE I
PERFORMANCE FOR ONE-PHASE OPEN FAULT

Conditions	Healthy	Fault	M_1	M_2	M_3	M_4
ρ	1.00	1.82	1.00	1.00	1.61	1.52
$\Delta T_e(\%)$	2.1	23.1	4.4	20.2	3.5	5.3

The remaining stator currents are unbalanced, and each phase copper loss is different. Stator current equalization is expressed

$$\rho = \frac{\max(I'_b, I'_c, I'_d, I'_e)}{\min(I'_b, I'_c, I'_d, I'_e)}. \tag{28}$$

Torque ripple is a key value for drive system, and the aim of fault-tolerant control is to reduce the pulsation. The parameter is defined as

$$\Delta T_e = \frac{T_{e(\max)} - T_{e(\min)}}{T_{e(\text{avg})}}. \tag{29}$$

The performances for one-phase open fault are listed in Table I. The stator currents are balanced distributed in the M_1 and M_2 method, compared with M_3 and M_4 method. However, the torque pulsation is deteriorated in the M_2 method, because the third harmonic generates torque ripple in the fundamental spatial plane. Hence, the M_3 and M_4 method are proposed to reduce torque ripple even under harmonic current injection condition.

C. Two-Phase Open Fault

The experimental results under two-phase open fault condition are shown in Fig. 17, when the stator current are sinusoidal. The load is reduce for 8 N·m, because the maximum stator currents are limited under two-phase open condition. The torque

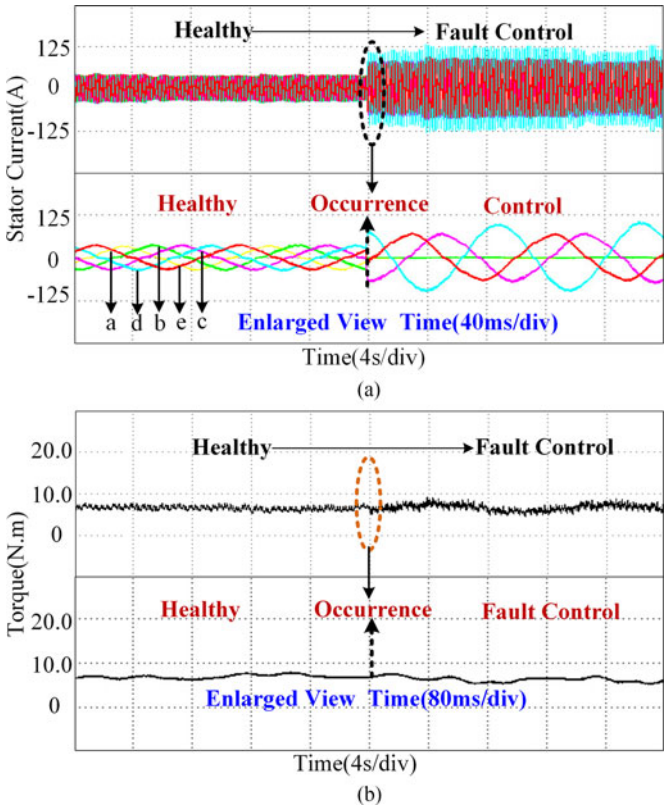

Fig. 17. Two-phase open fault result without third harmonic current injection (M_5). (a) Five-phase stator current. (b) Measured torque ripple.

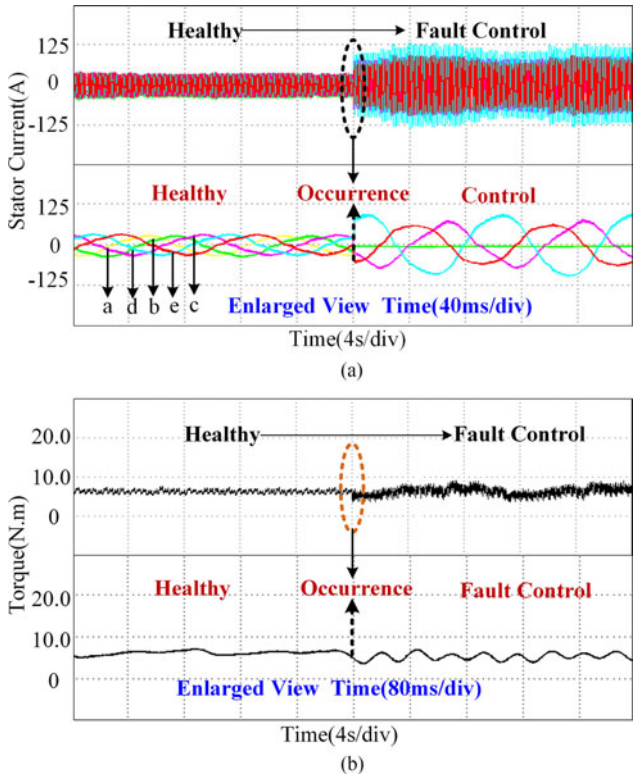

Fig. 18. Two-phase open fault result with third harmonic current injection for the traditional method (M_6). (a) Five-phase stator current. (b) Measured torque ripple.

performance in Fig. 17(b) indicates that the torque ripple remains smooth in the fault-tolerant condition.

The experimental results with third harmonic current injection for the traditional method are shown in Fig. 18. According to analysis in Section II, $\vec{i}^{3}_{S3}$ is circular trajectory, while $\vec{i}^{1}_{S3}$ is elliptical trajectory acted with larger inductance. Consequently, the torque ripple still remains large under fault-tolerant control condition shown in Fig. 18(b), and the percentage of pulsation amplitude is up to 17.2%. The angular frequency for torque ripple is 4ω, and the rotating direction is reverse resulting in high rotor loss.

The experimental results with third harmonic current injection for the proposed method are shown in Fig. 19. It should be noted that $\vec{i}^{3}_{S3}$ is elliptical trajectory, while $\vec{i}^{1}_{S3}$ is circular trajectory acted with fundamental inductance. The reverse component of current space vector $\vec{i}^{1}_{S3}$ is removed by the proposed method, and the torque ripple can be reduced obviously compared with the results in Fig. 19(b). The current space vector under two-phase open condition is shown in the Fig. 20, and $\vec{i}^{1}_{S3}$ is optimized for the circular trajectory to reduce the torque ripple. Hence, the fundamental and other harmonic currents mapped into fundamental spatial plane should remain circular, and the reverse MMF is required to be avoided.

The performances for two-phase open fault are listed in Table II. The torque ripple for the proposed method is reduced significantly compared with the traditional method. According to the values in the method M_6 and M_7, it is shown that third

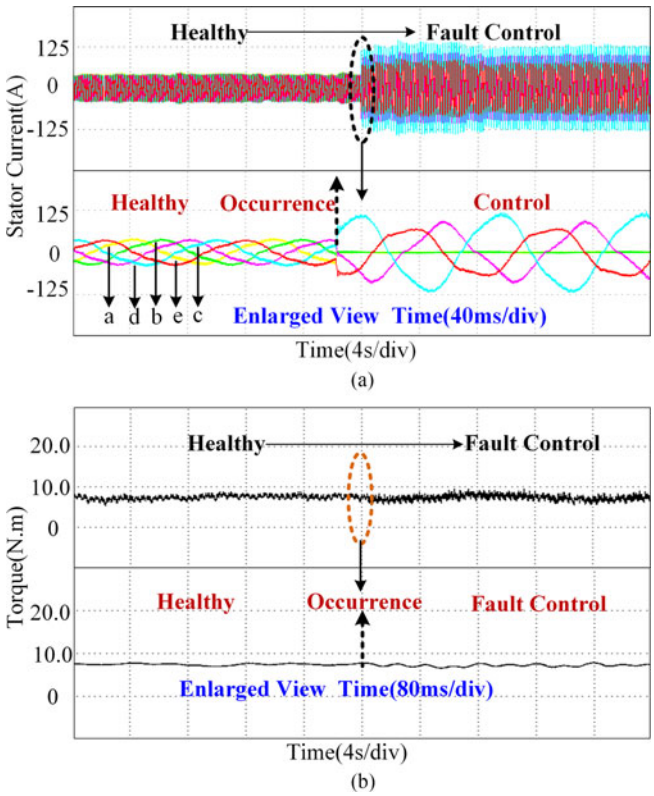

Fig. 19. Two-phase open fault result with third harmonic current injection for the proposed method (M_7). (a) Five-phase stator current. (b) Measured torque ripple.

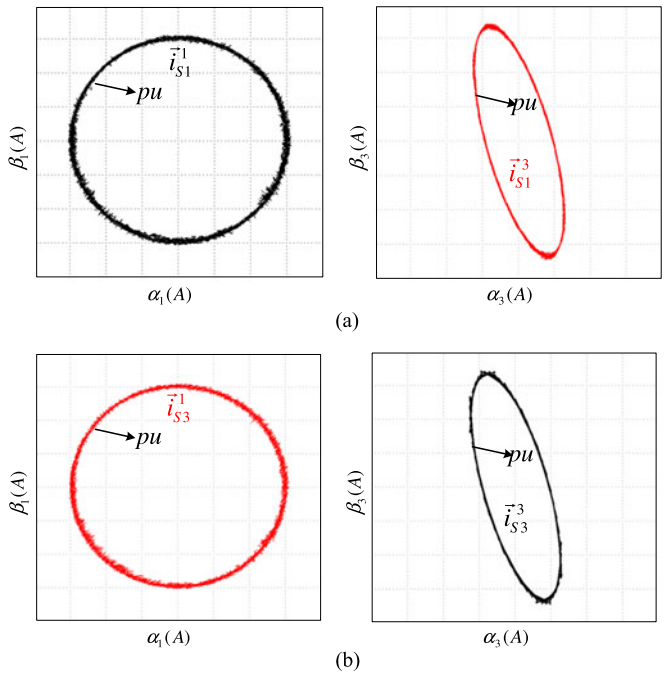

Fig. 20. Experimental results for the proposed method under two-phase fault condition. (a) Fundamental stator current space vector. (b) Third harmonic stator current space vector.

TABLE II
PERFORMANCE FOR TWO-PHASE OPEN FAULT

Conditions	Healthy	M_5	M_6	M_7
ρ	1.00	0.62	0.41	0.58
$\Delta T_e(\%)$	2.1	11.4	30.5	13.6

harmonic current is also can be used to improve the torque density even under two-phase open fault condition.

VI. CONCLUSION

This paper has investigated spatial harmonic magnetic field effects on torque ripple for multiphase IM with concentrated full pitch winding. The analytical formulation utilizes multiple current space vector representation, and the coupling of current space vector is presented between fundamental and harmonic planes. The stator currents are optimized to maintain the circular trajectory in the fundamental spatial plane, and it aims to generate high quality torque output. The negative effect caused by spatial magnetic field coupling can be diminished with suitable control method. To assess the effectiveness of the proposed method, four control strategies are compared under single-phase open condition. Moreover, it is proved that the proposed method can realize torque-ripple free under two-phase open condition. Furthermore, the PIR controller is optimized, and different values of parameters in the transfer function are derived. The fault-tolerant strategies demonstrate that multiphase motor can continue to operate with a rotating as long as no more than (n–3) phases are faulted. Finally, the proposed method is further validated by experiments.

APPENDIX

TABLE III
PARAMETERS OF FIVE-PHASE IM

Rated power	5 kW	L_{m3}	0.18 mH
Current (RMS)	73 A	$L_{or1} \approx L_{or3}$	0.03 mH
Torque	25 N·m	$L_{os1} \approx L_{os3}$	0.02 mH
Poles	2	R_s	0.011 Ω
Rated speed	1940 (r/min)	R_{r1}	0.009 Ω
L_{m1}	1.58 mH	R_{r3}	0.008 Ω

REFERENCES

[1] E. Levi, "Multiphase electric machines for variable-speed application," *IEEE Trans. Ind. Electron.*, vol. 55, no. 5, pp. 1893–1909, May 2008.
[2] E. Levi, R. Bojoi, F. Profumo, H. A. Toliyat, and S. Williamson, "Multiphase induction motor drives—A technology status review," *IET Electr. Power Appl.*, vol. 1, no. 4, pp. 489–516, Jul. 2007.
[3] F. Barrero and M. Duran, "Recent advances in the design, modeling and control of multiphase machines - Part 1," *IEEE Trans. Ind. Electron.*, vol. 63, no. 1, pp. 449–458, Jan. 2016.
[4] B. A. Welchko, T. A. Lipo, T. M. Jahns, and S. E. Schulz, "Fault tolerant three-phase AC motor drive topologies: A comparison of features, cost, and limitations," *IEEE Trans. Power Electron.*, vol. 19, no. 4, pp. 1108–1116, Jul. 2004.
[5] M. Benatmane and T. McCoy, "Development of a 19 MW PWM converter for U.S. Navy surface ships," in *Proc. Int. Conf. ELECSHIP*, Istanbul, Turkey, 1998, pp. 109–113.
[6] J. J. Simond, A. Sapin, T. Xuan, R. Wetter, and P. Burmeister, "12-pulse LCI synchronous drive for a 20 MW compressor: Modelling, simulation and measurements," in *Proc. 40th Int. Conf. IEEE Ind. Appl. Soc.*, Hong Kong, 2005, pp. 2302–2308.
[7] S. Z. Jiang, K. T. Chau, and C. C. Chan, "Spectral analysis of a new six-phase pole-changing induction motor drive for electric vehicles," *IEEE Trans. Ind. Electron.*, vol. 50, no. 1, pp. 123–131, Feb. 2003.
[8] X. Huang *et al.*, "Fault-tolerant brushless DC motor drive for electro-hydrostatic actuation system in aerospace application," *in Proc. 41st Int. Conf. IEEE Ind. Appl. Soc.*, Tampa, FL, USA, 2006, pp. 473–480.
[9] B. Ge, D. Sun, W. Wu, and F. Peng, "Winding design, modeling, and control for pole-phase modulation induction motors," *IEEE Trans. Magn.*, vol. 49, no. 2, pp. 898–911, Feb. 2013.
[10] L. Zheng, J. E. Fletcher, B. W. Williams, and X. He, "Dual-plane vector control of a five-phase induction machine for an improved flux pattern," *IEEE Trans. Ind. Electron.*, vol. 55, no. 5, pp. 1996–2005, May 2008.
[11] R. O. C. Lyra and T. A. Lipo, "Torque density improvement in a six phase IM with third harmonic current injection," *IEEE Trans. Ind. Appl.*, vol. 38, no. 5, pp. 1351–1360, Sep./Oct. 2002.
[12] K. Wang, Z. Z. Zhu, Y. Ren, and G. Ombach, "Torque improvement of dual three-phase permanent-magnet machine with third-harmonic current injection," *IEEE Trans. Ind. Electron.*, vol. 62, no. 11, pp. 6833–6844, Nov. 2015.
[13] R. R. Errabelli and P. Mutschler, "Fault-tolerant voltage source inverter for permanent magnet drives," *IEEE Trans. Power Electron.*, vol. 27, no. 2, pp. 500–508, Feb. 2012.
[14] B. Vaseghi, N. Takorabet, J. P. Caron, B. Nahid-mobarakeh, F. Meibody-Tabar, and G. Humbert, "Study of different architectures of fault-tolerant actuator using a two-channel PM motor," *IEEE Trans. Ind. Appl.*, vol. 47, no. 1, pp. 47–54, Jan./Feb. 2011.
[15] H. Xu, H. A. Toliyat, and L. J. Petersen, "Rotor field oriented control of a five-phase induction motor with the combined fundamental and third harmonic currents," in *Proc. 16th Int. Conf. IEEE Appl. Power Electron.*, Anaheim, CA, USA, 2001, vol. 1, pp. 392–398.
[16] H. A. Toliyat, L. Parsa, and N. Bianchi, "Resilient current control of five-phase induction motor under asymmetrical fault," in *Proc. 17th Annu. Conf. IEEE Appl. Power Electron.*, Dallas, TX, USA, 2002, vol. 1, pp. 64–71.
[17] Y. Zhao and T. A. Lipo, "Modeling and control of a multi-phase induction machine with structural unbalance—Part I: Machine modeling and multidimensional current regulation," *IEEE Trans. Energy Convers.*, vol. 11, no. 3, pp. 570–577, Sep. 1996.

[18] Y. Zhao and T. A. Lipo, "Modeling and control of a multi-phase induction machine with structural unbalance—Part II: Field-oriented control and experimental verification," *IEEE Trans. Energy Convers.*, vol. 11, no. 3, pp. 578–584, Sep. 1996.
[19] H. Ryu, J. Kim, and S. Sul, "Synchronous-frame current control of multiphase synchronous motor under asymmetric fault condition due to open phases," *IEEE Trans. Ind. Appl.*, vol. 42, no. 4, pp. 1062–1070, Jul./Aug. 2006.
[20] R. Kiani-Nezhad, B. Nahidmobarakeh, L. Baghli, F. Betin, and G. A. Capolino, "Modeling and control of six-phase symmetrical induction machines under fault condition due to open phases," *IEEE Trans. Ind. Electron.*, vol. 55, no. 5, pp. 1966–1977, May 2008.
[21] A. S. Abdel-Khalik, M. A. Elgenedy, S. Ahmed, and A. M. Massoud, "An improved fault-tolerant five-phase induction machine using a combined star/pentagon single layer stator winding connection," *IEEE Trans. Ind. Electron.*, vol. 63, no. 1, pp. 618–628, Jan. 2016.
[22] S. Dwari and L. Parsa, "Fault-tolerant control of five-phase permanent magnet motors with trapezoidal back EMF," *IEEE Trans. Ind. Electron.*, vol. 58, no. 2, pp. 476–485, Feb. 2011.
[23] A. Mohammadpour and L. Parse, "A unified fault-tolerant current control approach for five-phase PM motors with trapezoidal back EMF under different stator winding connections," *IEEE Trans. Power Electron.*, vol. 28, no. 7, pp. 3517–3527, Jul. 2013.
[24] A. Mohammadpour, S. Sadeghi, and L. Parsa, "A generalized fault-tolerant control strategy for five-phase PM motor drives considering star, pentagon, pentacle connections of stator windings," *IEEE Trans. Ind. Electron.*, vol. 61, no. 1, pp. 63–75, Jan. 2014.
[25] A. Tani, M. Mengoni, L. Zarri, G. Serra, and D. Casadei, "Control of multiphase induction motors with an odd number of phase under open-circuit phase faults," *IEEE Trans. Power Electron.*, vol. 27, no. 2, pp. 565–577, Jul. 2012.
[26] D. Jiang and F. Wang, "A general current ripple prediction method for the multiphase voltage source converter," *IEEE Trans. Power Electron.*, vol. 29, no. 6, pp. 2643–2648, Jun. 2014.
[27] D. G Holmes, T. A. Lipo, B. P. McGrath, and W. Y. Kong, "Optimized design of stationary frame three phase AC current regulators," *IEEE Trans. Power Electron.*, vol. 24, no. 11, pp. 2417–2426, Nov. 2009.
[28] D. G. Holmes, B. P. McGrath, and S. T. Parker, "Current regulation strategies for vector-controlled induction motor drives," *IEEE Trans. Ind. Electron.*, vol. 59, no. 10, pp. 3680–3688, Oct. 2012.
[29] H. Guzman, M. J. Duran, F. Barrero, B. Bogado, and S. Toral, "Speed control of five-phase induction motors with integrated open-phase fault operation using predictive current techniques," *IEEE Trans. Ind. Electron.*, vol. 61, no. 9, pp. 4474–4484, Sep. 2014.
[30] C. S. Lim, E. Levi, M. Jones, N. A. Rahim, and W. P. Hew, "FCS-MPC based current control of a five-phase induction motor and its comparison with PI-PWM control," *IEEE Trans. Ind. Electron.*, vol. 61, no. 1, pp. 149–163, Jan. 2014.
[31] H. S. Che, M. J. Duran, E. Levi, W. Hew, and N. Abd. Rahim, "Postfault operation of an asymmetrical six-phase induction machine with single and two isolated neutral points," *IEEE Trans. Power Electron.*, vol. 29, no. 10, pp. 5406–5416, Oct. 2014.

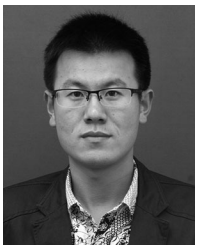

Wubin Kong (M'15) was born in Zhejiang, China, in 1986. He received the B.S. and Ph.D. degrees in power electronics and motor drives from Zhejiang University, Hangzhou, China, in 2009 and 2014, respectively.

Since 2015, he has been a Lecture with Huazhong University of Science and Technology, Wuhan, China. His research interests include high-power multiphase motor drives and fault tolerant control motor drive applied in EV.

Min Kang received the B.S. and Ph.D. degrees in power electronics and motor drives from the College of Electrical Engineering, Zhejiang University, Hangzhou, China, in 2003 and 2008, respectively.

From 2008 to 2011, he was a Lecturer in the College of Electrical Engineering, Zhejiang University of Science and Technology, Hangzhou. He is currently an Associate Professor in the Zhejiang of Science and Technology. His research interests include mul-

Dawei Li (S'12–M'15) was born in China. He received the B.E.E. degree in power electronics and motor drives from Harbin Institute of Technology, Harbin, China, in 2010, and the Ph.D. degree in electrical engineering from Huazhong University of Science and Technology, Wuhan, China, in 2015.

In July 2015, he joined Huazhong University of Science and Technology, Wuhan. His research interests include the design and analysis of flux-modulation permanent-magnet brushless machines.

Dr. Li received the Best Poster Presentation Award from the XXII-th International Conference on Electrical Machines (ICEM 2016), and Hubei Province Excellent Doctoral Dissertation (2016), China. He has authored more than 60 published technical papers and is the holder of more than ten patents/patent applications.

Ronghai Qu (S'01–M'02–SM'05) was born in China. He received the B.E.E. and M.S.E.E. degrees in power electronics and motor drives from Tsinghua University, Beijing, China, in 1993 and 1996, respectively, and the Ph.D. degree in electrical engineering from the University of Wisconsin-Madison, Madison, WI, USA, in 2002.

In 1998, he joined the Wisconsin Electric Machines and Power Electronics Consortiums as Research Assistant. He became a Senior Electrical Engineer with Northland, a Scott Fetzer Company in 2002. Since 2003, he has been with the Electrical Machines and Drives Laboratory, General Electric (GE) Global Research Center, Niskayuna, NY, USA, as a Senior Electrical Engineer. Since 2010, he has been a Professor with Huazhong University of Science and Technology, Wuhan, China.

Dr. Qu has authored more than 50 published technical papers and is the holder of more than 40 patents/patent applications. He is a full member of Sigma Xi. He has been receiving several awards from GE Global Research Center since 2003, including the Technical Achievement and Management Awards. He also received the 2003 and 2005 Best Paper Awards, third prize from the Electric Machines Committee of the IEEE Industry Applications Society at the 2002 and 2004 IAS Annual Meeting.

Dong Jiang (S05'–M12'–SM16') received the B.S. and M.S. degrees in electrical engineering from Tsinghua University, Beijing, China, in 2005 and 2007, respectively. He began the Ph.D. degree in the Center for Power Electronics Systems, Virginia Tech, Blacksburg, VA, USA, in 2007, and was transferred to the University of Tennessee, Knoxville, TN, USA, with his advisor in 2010. He received the Ph.D. degree in power electronics and motor drives from the University of Tennessee, Knoxville, TN, in December 2011.

He was with the United Technologies Research Center, East Hartford, CT, USA, as a Senior Research Scientist/Engineer from January 2012 to July 2015. Since July 2015, he has been with Huazhong University of Science and Technology, Wuhan, China as a Professor. His major research interests include power electronics and motor drives, with more than 40 published IEEE journal and conference papers in this area.

Dr. Jiang received two Best Paper Awards in IEEE conferences. He is an Associate Editor of the IEEE TRANSACTIONS ON INDUSTRY APPLICATIONS.

Chun Gan (S'14–M'16) received the B.S. and M.S. degrees in power electronics and motor drives from China University of Mining and Technology, Jiangsu, China, in 2009 and 2012, respectively, and the Ph.D. degree in power electronics and motor drives from Zhejiang University, Hangzhou, China, in 2016.

He is currently a Research Associate with the Department of Electrical Engineering and Computer Science, University of Tennessee, Knoxville, TN, USA. He is also a member of the U.S. Energy/National Science Foundation cofunded Engineering Research Center CURENT. He has published more than 40 technical papers in leading journals and conference proceedings, and authored one book chapter. He has ten issued/published invention patents. His research interests include high-efficiency power converters, electric vehicles, electrical motor drives, electrical motor design, continuous variable series reactor, high voltage direct current transmission, and microgrid.

Dr. Gan received the 2015 Top Ten Excellent Scholar Award, the 2016 Excellent Ph.D. Graduate, the 2015 Ph.D. National Scholarship, the 2015 Wang Guosong Scholarship, and the 2014 and 2015 Outstanding Ph.D. Candidate in